Wormhole Forward Modeling and Seismic Responses

Xiaoqin Cui*, CHORUS, Department of Geoscience University of Calgary, Canada
xicui@ucalgary.ca
and
Laurence R. Lines, Edward S. Krebes and Joan Embleton, Department of Geoscience, University of Calgary, Canada

Summary

Wormholes form several fractural networks leading to the increased reservoir permeability in cold heavy oil production with sand (CHOPS). We can extend the linear slip theory (Schoenberg, 1980) and generalized homogeneous finite difference approach (Korn and Stockl, 1982) with the fracture parameters to model the wormholes in CHOPS and the recorded synthetic seismograms from the wormholes. This paper illustrates that the seismic characters, such as amplitude, frequency, and travel time (velocity) will vary with the fractural network wormhole features. Also, the paper exhibits that 4D seismic time-lapse technology can be used to monitor CHOPS production.

Introduction

The fact is that more than 50 percent of Canada's oil production is from heavy oil production (Batzle et al., 2006), therefore, the comprehensive method of the economical recovery and production monitoring are significantly important. One of the popular heavy oil recovery methods is known as CHOPS (cold heavy oil production with sand) in which the reservoir maintains at a constant temperature rather than experiencing increasing temperatures for the purpose of reducing heavy oil viscosity during the process of thermal heavy oil production. Cold production is normally suited to lowering viscosity and the interfacial tension for the thin pay zone of 10 meters or less. During the cold production process, sand, oil, water, and gas are produced simultaneously by using progressive cavity pumps which generate high-porosity fractal network (channels) termed as "wormholes"(Lines et al., 2003). Figure 1 shows a pattern of wormhole growth that looks like the fractal root system of a plant - that has random directions of fractures in a pay zone (Yuan et al., 1999). Thus, in the pay zone, in the x-y plane (horizontal plane), the wormholes that can be imaged as a layer in which the numbers of the fractures in the near central zone are less dense than at the edges of the wormhole zone. In the x-z plane (vertical plane), the fractures have a shape as shown in Figure 2. Therefore, the elastic wave propagation through different parts of the 3D wormhole network will have different responses to be recorded in a seismogram. A 3D finite difference (FD) scheme is considered to work for the wormhole forward modeling.

Theory and/or Method

In 1980, Schoenberg gave a linear slip interface theory: a fracture is modeled as a non-welded contact (linear slip) interface where the particle displacements are discontinuous across the interface and the stresses are continuous across it. The particle displacements are linearly proportional to the stresses. From his pioneering work, the compliances of the fracture parameter η are elicited in the boundary condition. For example, in the VTI medium, if one horizontal fracture can be modeled as a horizontal non-welded interface,

$$\boldsymbol{\varphi}^{+} - \boldsymbol{\varphi}^{-} = \boldsymbol{\eta}\boldsymbol{\sigma}$$
$$\boldsymbol{\sigma}^{-} = \boldsymbol{\sigma}^{+}$$

Where $\boldsymbol{\varphi} = \begin{bmatrix} u_x \\ v_y \\ w_z \end{bmatrix}$, $\boldsymbol{\eta} = \begin{bmatrix} \eta_t & 0 & 0 \\ 0 & \eta_t & 0 \\ 0 & 0 & \eta_N \end{bmatrix}$, $\boldsymbol{\sigma} = \begin{bmatrix} \sigma_{xz} \\ \sigma_{yz} \\ \sigma_{zz} \end{bmatrix}$. $\boldsymbol{\varphi}$ represents wave motion three components as u_x, v_y and w_z respectively. $\boldsymbol{\sigma}$ denotes normal (σ_{zz}) and shear (σ_{xz},σ_{yz}) tractions of the motion. The signs of the plus and minus represent the upper (left) and lower (right) medium at the interface or the fracture, respectively. $\boldsymbol{\eta}$ is termed the fracture parameter. η_N is the normal compliance for the normal incident compressional wave and η_t is tangential compliance for a normal incident shear wave. η_N and η_t are orthogonal to each other. In other words, η_t is parallel to the polarization of the shear wave and perpendicular to the polarization of the compressional wave, and vice-versa for η_N .The directions of the fracture and wave polarization are very critical factors and play an integral part in the forward modeling of the wormholes, because the wormhole exhibits random interleaving of the horizontal and vertical fractures that have been impinged by the different wave PP and PS. Let us separate the fracture system into pure x- fracture only once the fracture's tangential compliance parallel in the x axis, and pure y-fracture meaning the tangential compliance are parallel to the y axis, therefore, the wormhole can be simply decomposed into pure x-fractures and pure y- fractures in the x-y plane that are projected vertical fractures in the x-z plane or the y-z plane that tangential compliance takes the unchanged values along the z direction or thickness of the pay zone.

In 1982, Korn and Stockl presented a 2D that generalized the homogeneous approach in which the fictitious grid points are introduced to extend one medium into the nearest-neighbor medium in order to model the SH wave propagation through a boundary. In 2000, Slawinski and Krebes used the 2D generalized homogeneous approach to model SH and P-SV wave propagation in nonwelded contact interface as a horizontal fracture. This FD scheme of wave motion with the fictitious grid points takes more physical insight into to the fracture forward modeling in that the medium and boundary conditions (BCs) that has a imposed explicitly. In other words, the equation of motion governs the motion outside of the discontinuity interface (fracture), but non-welded contact boundary condition is applied at the discontinuity interface. In the 3D domain, the fractures are represented as interfaces and are satisfying the discontinuity of displacement and continuity traction BCs across interfaces at (x$\mp$1/2, y, z), (x, y$\mp$1/2, z), (x, y, z$\mp$1/2) respectively. Let us define the dimensionless non-weldedness parameters (Slawinski, 1999). $\varepsilon_x^y = \frac{\mu\eta_N}{h}$, $\varepsilon_y^y = \frac{\mu\eta_t}{h}$ and $\emptyset = \frac{(\lambda+2\mu)\eta_t}{h}$ are for the pure y-fracture. $\varepsilon_x^x = \frac{\mu\eta_N}{h}$, $\varepsilon_y^x = \frac{\mu\eta_t}{h}$ and $\emptyset = \frac{(\lambda+2\mu)\eta_t}{h}$ are for the pure x-fracture. In 3D wave propagation, once the x-component wave motion propagate relatively to the direction of the y axis or y pure fractures, then η_N is orthogonal to the direction y and FD scheme associate withε_x^y, whereas η_t is orthogonal to η_N and FD scheme associated with ε_y^y in this time. Similarity, ε_x^x and ε_y^x are contribute to the pure x-fracture. Thus the FD scheme for a 3D wormhole equation is

$$\begin{aligned}\boldsymbol{\varphi}_{x,y,z}^{t+\Delta t} = {} & 2\boldsymbol{\varphi}_{x,y,z}^{t} - \boldsymbol{\varphi}_{x,y,z}^{t-\Delta t} + \frac{1}{\rho}\left(\frac{\Delta t}{h}\right)^2 \{\mathbf{A}_f(\boldsymbol{\varphi}_{x+\Delta x,y,z}^{t} - 2\boldsymbol{\varphi}_{x,y,z}^{t} + \boldsymbol{\varphi}_{x-\Delta x,y,z}^{t}) + \\ & \mathbf{B}_f(\varphi_{x,y+\Delta y,z}^{t} - 2\boldsymbol{\varphi}_{x,y,z}^{t} + \boldsymbol{\varphi}_{x,y-\Delta y,z}^{t}) + \mathbf{C}_f(\boldsymbol{\varphi}_{x,y,z+\Delta z}^{t} - 2\boldsymbol{\varphi}_{x,y,z}^{t} + \boldsymbol{\varphi}_{x,y,z-\Delta z}^{t}) + \\ & \frac{1}{4}\mathbf{D}_f\left(\boldsymbol{\varphi}_{x+\Delta x,y+\Delta y,z}^{t} - \boldsymbol{\varphi}_{x+\Delta x,y-\Delta y,z}^{t} - \boldsymbol{\varphi}_{x-\Delta x,y+\Delta y,z}^{t} + \boldsymbol{\varphi}_{x-\Delta x,y-\Delta y,z}^{t}\right) + \\ & \frac{1}{4}\mathbf{E}_f\left(\boldsymbol{\varphi}_{x+\Delta x,y,z+\Delta z}^{t} - \boldsymbol{\varphi}_{x+\Delta x,y,z-\Delta z}^{t} - \boldsymbol{\varphi}_{x-\Delta x,y,z+\Delta z}^{t} - \boldsymbol{\varphi}_{x-\Delta x,y,z-\Delta z}^{t}\right) + \\ & \frac{1}{4}\mathbf{F}_f\left(\boldsymbol{\varphi}_{x,y+\Delta y,z+\Delta z}^{t} - \boldsymbol{\varphi}_{x,y+\Delta y,z-\Delta z}^{t} - \boldsymbol{\varphi}_{x,y-\Delta y,z+\Delta z}^{t} + \boldsymbol{\varphi}_{x,y-\Delta y,z-\Delta z}^{t}\right)\}.\end{aligned}$$

Where,$\mathbf{A}_f$, $\mathbf{B}_f$,$\mathbf{C}_f$, $\mathbf{D}_f$, $\mathbf{E}_f$,$\mathbf{F}_f$ are described byCui et al. (2012).

Examples

We have implemented a Matlab code for the forward modeling of the wormholes. In practical uses, it raises a question about the velocity variation with azimuth of the developed wormholes because its fractural network has formed an azimuthal anisotropic medium embedded in the initial isotopic homogeneous medium. But the velocity changes are ignored in this wormhole study in this paper. The values of the normal and tangential compliances of the fracture parameter are 0.025 and 0.049 in any kind of fracture respectively. Figure 3 illustrates the 3D synthetic seismic data response on the numerical wormhole model.

In general, when the seismic wave propagates in a fractured medium, waves are polarized parallel to the direction of the fracture travel with a fast velocity, otherwise, while waves polarized perpendicular to the direction of the fracture travel with a slow velocity. Figure 4 exhibits trace 1 as it passes through a non-fractured medium, and trace 2 is from the fractural wormhole (the pure horizontal fracture). It is clear that the x and z components have similar amplitudes for trace 1 and trace 2, and the velocity of trace 2 is faster than that of trace 1 (Red line illustrates) because trace 2 is polarized parallel to the direction of the fracture for both x and z components in the wormhole. Whereas trace 2 in the y component is polarized perpendicular to the direction of the fracture so that it relatively has lower velocity and has weaker amplitude compared to trace 1.

Seismic wave manifests the frequency dispersion when it propagates into the fracture, which means that the velocity of the propagating wave depends on its frequency. Figure 5 presents two traces from the non-fracture area (left) and the wormhole (right) respectively. The velocity is independent of frequency for the trace from the non-fracture area (left). The velocity varies with the frequency for the trace from the fractured area.

The time lapse method can identify the wormhole geometrical shape. Figure 6 shows the subsurface models (black, bottom) and the time slice of the synthetic seismic data. Obviously, 4D seismic data from wormholes can be used to avoid invalid drilling and monitor production. In Figure 7, the x-component data provides additional information to regarding the developed wormhole.

Conclusions

A generalized homogeneous finite-difference method is extended and combined with the non-welded contact interface theory for the 3D seismic modeling of wormhole features. Synthetic seismic data as affected by wormholes demonstrate the azimuthal anisotropy and frequency dispersion. Time-lapse synthetic data illustrates the effects of wormhole growth and is used to evaluate the reservoir permeability in enhanced oil & gas recovery.

Acknowledgements

We would like to thank the sponsors of CHORUS. Thanks to Ge Zhan and Peng Cheng for discussion of the Matlab coding.

References

Cui, X.Q., Lines, L.R., and Krebes, E.S., 2012, Cold heavy oil reservoir characterization: wormhole modeling and seismic responses: CREWES Research Report –Volume 24.

Batzle, M., and Hofmann, R., 2006, Heavy oils—seismic properties: The Leading Edge, June, 2006.

Lines, L.R., Chen, S., Daley, P.F., and Embleton, J., 2003, Seismic pursuit of wormholes: The Leading Edge, 22, 459-461.

Slawinski, Raphael A., 1999, Finite-difference modeling of SH-wave propagation in nonwelded contact media: Geophysics, vol 67, No5.

Slawinski, Raphael A., and Krebes, Edward S., 2000, Finite-difference modeling of SH-wave propagation in nonwelded contact media: Geophysics, vol 67, No5.

Schoenberg, M., 1980, Elastic wave behavior across linear slip interfaces:J. Acoust. Soc. Am., 68, 1516-1521.

Yuan, J.Y., Tremblay, B., and Babchin, A., 1999, A wormhole network model of cold production in heavy oil: SPE Paper 54097.

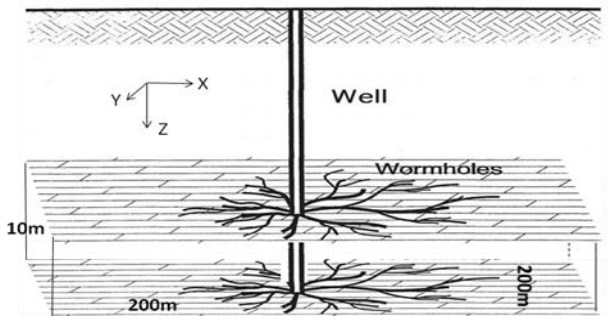

Figure 1: A schematic of a 3D wormhole model (Modified Miller et al, 1999).

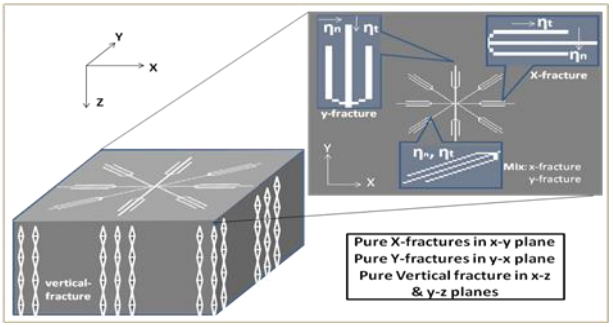

Figure 2: Numerical wormhole separates into pure x, y and vertical fracture.

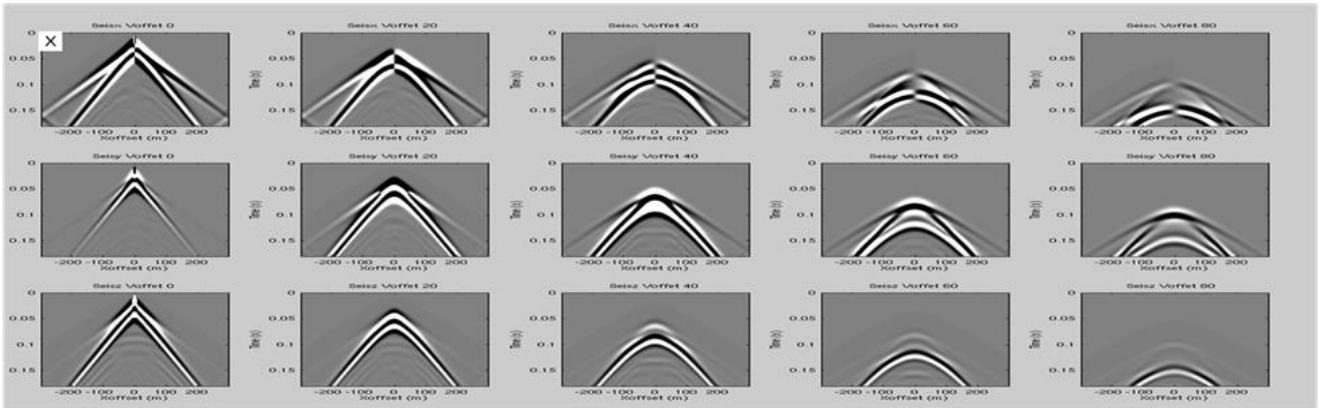

Figure 3: Three components x (top), y (middle) and z (bottom) synthetic seismograms response a wormhole. The geometry and all parameters are same as in Cui et al. (2012).

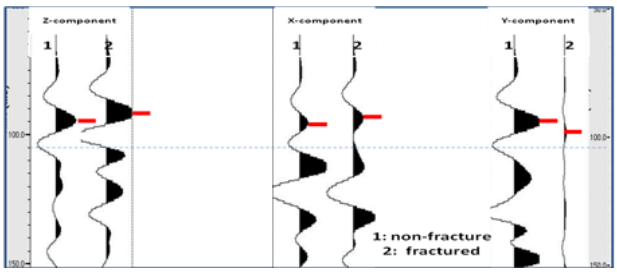

Figure 4: Seismic trace amplitude and velocity (travel time) variations respect to the direction of the fracture.

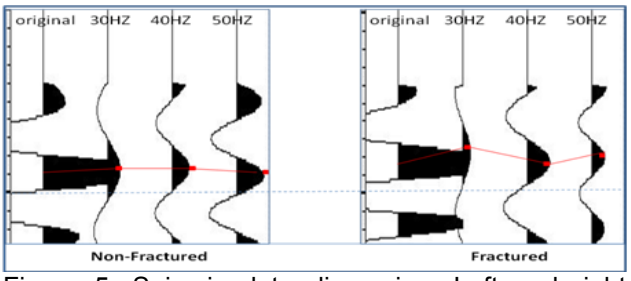

Figure 5: Seismic data dispersion. Left and right show traces from the non-fracture and fractured area respectively.

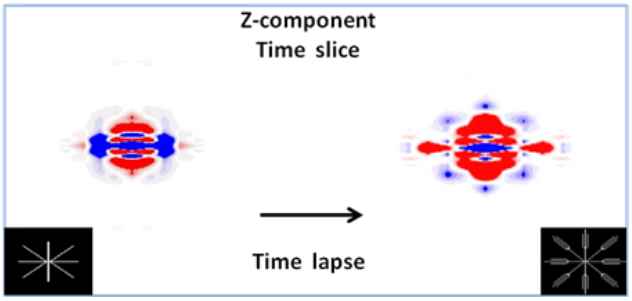

Figure 6: z-component time lapse show shapes and sizes of the wormhole.

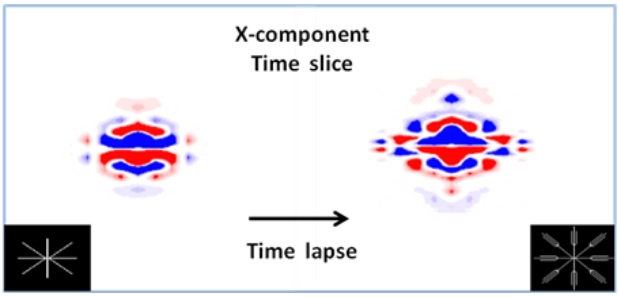

Figure 7: x-component time lapse show shapes and sizes of the wormhole.